Available online at www.sciencedirect.com
ScienceDirect
International Journal of Thermal Sciences 47 (2008) 306–314
International Journal of Thermal Sciences
www.elsevier.com/locate/ijts

Study on liquid-jet cooling and heating of the moving SMA actuator

Li-xiang Zhang *, Guo-xin Hu, Zhi-guo Wang

School of Mechanical & Power Engineering, Shanghai Jiaotong University, 200240 Shanghai, China

Received 14 November 2006; received in revised form 28 February 2007; accepted 1 March 2007

Available online 5 April 2007

Abstract

In this paper the numerical simulation and experiment were performed to investigate liquid-jet cooling and heating of the moving SMA (shape memory alloy). Two-dimensional unsteady flow was solved using the laminar flow model and energy conservation equation. The solid region was simulated by coupling the fluid with moving boundary and static boundary condition at the fluid–solid interface, respectively. Results showed that separation on the moving SMA surface was observed for the heating process and some vortices away from the moving surface were induced for the cooling process. A subatmospheric region on the impingement surface was observed with the increase of the streamwise distance from the stagnation point. The temperature of SMA actuator was compared for static and moving surface at different exit velocities, jet periods and nozzle-to-surface distances. The shape deformation of the actuator increased with the increase of the jet velocity and period, decreased with the increase of the nozzle-to-surface distance. An experiment on jet impingement was set up to study the liquid-jet cooling and heating the SMA actuator. The results of the numerical simulation were in good agreement with the experimental data.

Keywords: Liquid-jet; SMA actuator; Impingement heat transfer; Moving/static boundary condition

1. Introduction

With the development of the microelectromechanical systems (MEMS), a great deal of attention has been paid to the functional materials as the key component of the actuator. SMA, as a kind of functional material, possesses many desirable properties: high power to weight ratio, the ability to recover large transformation stress and strain upon heating and cooling, pseudoelasticity, high damping capacity, good chemical resistance, biocompatibility and fatigue properties [1,2]. However, SMA used as the actuator has a drawback of lower response frequency due to the deficiency of heat transfer, so it is hard to satisfy the situation of higher actuated frequency requirement. Jet impingement technique has been applied to a variety of production processes including the drying of papers and textiles, the tempering of glass, the postprocessing of some metals due to its effective heat and mass transfer performance, in particular this jet impingement cooling has been effectively used to eliminate excessive thermal load near the leading edge of the inner surface of gas turbine blades and the outer wall of combustors [3–7]. The study on cooling of high heat flux surface in fusion reactor by impinging planar jet flow was reviewed by Inoue et al. [8–10]. Bintoro et al. [11] reported designing and testing of a closed-loop electronics cooling system that adopts bi-technologies: single phase impinging jet and mini channels heat exchanger. They got the conclusion that cooling system developed in their paper was ready for cooling application inside a desktop and/or super computer.

SMA has been applied to the macroscale over the last several decades. However, its application to microelectromechanical systems (MEMS) started in the early 1990s when Walker et al. [12] fabricated a SMA coil spring on a silicon wafer to demonstrate the compatibility of thin film NiTi with MEMS fabrication process. Since that initial work, many research studies have been conducted on integrating sputter-deposited thin-film SMA into microdevices. Rediniotis et al. [13] fabricated a SMA biomimetic hydrofoil, which was able to deform several shape mimicking aquatic swimming. Lau et al. [14] demonstrated an application of SMA composite for active structural motion control of a clamped–clamped graphite/epoxy bean with embedded SMA actuator at the neutral axis. The applica-

* Corresponding author.
E-mail address: zhanglixiang@sjtu.edu.cn (L.-x. Zhang).

1290-0729/$ – see front matter
doi:10.1016/j.ijthermalsci.2007.03.001

Nomenclature

a	correction coefficient of temperature	
A	austenitic finish temperature	K
b	correction coefficient of stress	
c	equivalent transition coefficient of stress and temperature	
c_M	equivalent transition coefficient of stress and temperature	
C	specific heat	J/kg°C
C_p	pressure coefficient	
D	width of the jet exit	m
F	shape deformation	m
L	distance from jet exit to SMA	m
L/D	nozzle-to-surface distance	
M	martensitic finish temperature	K
Nu	Nusselt number	
p	pressure	Pa
p_{max}	maximum pressure	Pa
p_0	atmosphere	Pa
t	time	s
x/D	streamwise distance from the stagnation point	
T	jet period	s
u	velocity in x coordinates	m/s
v	velocity in y coordinates	m/s
x, y	coordinates	m

Greek symbols

α	thermal diffusivity	m^2/s
θ	temperature	K
σ	stress	Pa
ξ	martensitic fraction	
ρ	density of water	Kg/m^3
λ	heat transfer conductivity	W/mK
υ	coefficient of kinematic viscosity	m^2/s

Subscript

A	austenitic
f	finish
L	water
M	martensitic
s	start
S	shape memory alloy

tion of the SMA reinforced composite was in structural acoustic radiation control, which was investigated by Humbeeck [15]. Baz and Tampia [16] have shown that discrete SMA actuator can be used to control buckling of flexible structure. Makino et al. [17] have developed a SMA actuated micropump as a component for use in micro analysis or micro dosage systems; the NiTi thin film is about 6 mm in thickness. Shin et al. [18] have developed a compact actuator pump generating high output force at large velocities by thin film (10 μm) nickel–titanium (NiTi) SMA. Kohl et al. [19] has developed a microgripper system which consists of a monolithic SMA device of 2 mm × 5.8 mm × 0.23 mm size and an integrated optical position sensor.

Some works dealing with the response of the SMA have been reported in recent years. Bhattacharyya et al. [20] reported the influence of the material parameters on the thermal response of the SMA using the numerical method. They found that for short wires, the assumption of constant thermal conductivity underestimated the actuation and overestimated the cycle time significantly, that for long wires, the thermal conductivity effect was diminished whereas the electrical resistivity effect was very similar to that for the short wires. Ghomshei et al. [21] reviewed nonlinear transient response of a thick composite beam with SMA layers and demonstrated the effects of different material and geometric properties on the active vibration response of the SMA composite beam. Lagoudas and Bhattacharyya [22] presented numerical results for the response of the SMA actuator by thermoelectrical method and indicated that thin SMA layer (≈6 μm thick) under partial phase transformation was capable of delivering frequencies of 30 Hz. Rohde and Schüssler [23] reviewed the response-time behaviour of laser micromachined NiTi SMA actuators. They not only reported the relationship of the heat capacity, electrical resistivity and thermal conductivity with temperature, but also reported the transient temperature of the SMA with time under laser heating and cooling process. In this paper the numerical simulation and experiment were used to investigate liquid-jet cooling and heating the moving SMA. The objective of this paper was to investigate the flow field, the pressure distribution for static and moving boundary condition and the effects of v_{in}, L/D and T on the heat transfer characteristic between the fluid and solid region.

2. Theoretical model

A schematic diagram of jet impingement heating and cooling the SMA actuator is shown in Fig. 1. A downward directed slot jet is placed symmetrically at the middle of the top surface of the domain. The flow is assumed to be two-dimensional, unsteady, incompressible, and laminar in Cartesian coordinate. The actuator heated and cooled by the jet liquid would flutter periodically. Its behavior is controlled by a constitutive equation developed by Liang and Logers [24]. The width of the jet is $D = 0.4$ mm; the jet liquid is water. The control area is assumed to be large enough to eliminate the influence of the solid wall and the pressure exit of the flow. The jet impingement on the SMA actuator is a complex process; some assumptions and simplifications must be taken for developing this model:

(1) The behavior of the SMA actuator is only a function of temperature.
(2) Constant properties are assumed in the solid region (SMA actuator).
(3) Inlet flow is uniform.

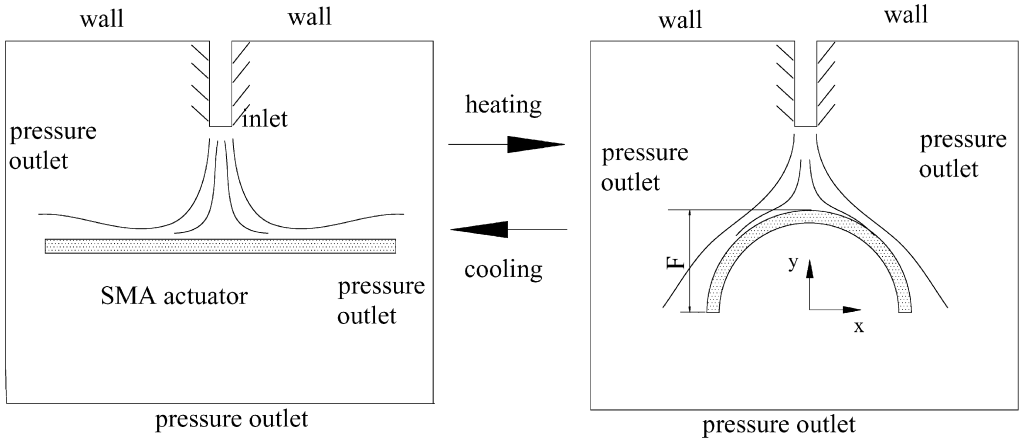

Fig. 1. Schematic diagram of simulation model.

(4) Viscous dissipation effects are neglected in the energy equation.

The top wall is simulated as a solid surface; the non-slip condition is applied. All the other surfaces of the controlled area are assumed as pressure outlets. No slip and convective boundary conditions are imposed at the conjugated interface between the water and the SMA actuator (fluid–solid interface).

Numerical solution of the above model is obtained using a finite-volume method, together with a finite-element approach of representing of the geometry. Dynamic meshes are adopted in the numerical solution; the location of the SMA actuator is updated for each iteration. The SIMPLE algorithm is used to solve the heat transfer and fluid flow problem. The calculations are done by an implicit Bachward–Euler scheme; the time step is 0.005 s. The convergence standard for momentum equation and the energy equation is 10^{-5} and 10^{-8}, respectively.

The governing equations are as follows:

- Continuity equation:

$$\frac{\partial u}{\partial x}+\frac{\partial v}{\partial y}=0 \tag{1}$$

- Momentum equation:

$$\frac{\partial u}{\partial t}+u\frac{\partial u}{\partial x}+v\frac{\partial u}{\partial y}=-\frac{\partial p}{\rho_{\mathrm{L}}\partial x}+\upsilon\left(\frac{\partial^2 u}{\partial x^2}+\frac{\partial^2 u}{\partial y^2}\right) \tag{2}$$

$$\frac{\partial v}{\partial t}+u\frac{\partial v}{\partial x}+v\frac{\partial v}{\partial y}=-\frac{\partial p}{\rho_{\mathrm{L}}\partial y}+g+\upsilon\left(\frac{\partial^2 v}{\partial x^2}+\frac{\partial^2 v}{\partial y^2}\right) \tag{3}$$

- The fluid energy equation:

$$\frac{\partial \theta_{\mathrm{L}}}{\partial t}+u\frac{\partial \theta_{\mathrm{L}}}{\partial x}+v\frac{\partial \theta_{\mathrm{L}}}{\partial y}=\alpha_{\mathrm{L}}\left(\frac{\partial^2 \theta_{\mathrm{L}}}{\partial x^2}+\frac{\partial^2 \theta_{\mathrm{L}}}{\partial y^2}\right) \tag{4}$$

- The SMA actuator energy equation:

$$\frac{\partial \theta_{\mathrm{S}}}{\partial t}=\alpha_{\mathrm{S}}\left(\frac{\partial^2 \theta_{\mathrm{S}}}{\partial x^2}+\frac{\partial^2 \theta_{\mathrm{S}}}{\partial y^2}\right) \tag{5}$$

The boundary conditions are:

(1) The jet exit:

$$v=v_{\mathrm{in}},\qquad u_{\mathrm{in}}=0$$

$$\theta_{\mathrm{in}}=f(t)=\begin{cases}353, & (nT)s\leqslant t\leqslant(n+0.5T)s\\ 283, & (n+0.5T)s\leqslant t\leqslant(n+T)s\\ & n=1,2,3,4\ldots\end{cases} \tag{6}$$

(2) The pressure outlet:

$$p=p_0,\qquad \theta=\theta_0 \tag{7}$$

(3) The solid wall:

$$u=v=0,\qquad \frac{\partial\theta}{\partial x}=\frac{\partial\theta}{\partial y}=0 \tag{8}$$

(4) The fluid–solid interface:
Zero velocities and continuity of convective heat-transfer coefficient are imposed at the fluid–solid interface. Convective heat-transfer coefficient of the liquid–solid interface is [25]

$$Nu_0=1.215Re^{0.4884}Pr_{1/3}(L/D)^{-0.0043} \tag{9}$$

$$\frac{Nu}{Nu_0}=\frac{1}{1+0.246x-0.022x^2} \tag{10}$$

The unique thermomechanical properties of SMA are due to a phase transformation from the austenite phase to the martensite phase or vice versa. To describe the behaviors of SMA, a variety of models have been developed. Liang and Logers [24] have developed a constitutive equation based on a cosine model to represent the martensite fraction. To begin with, we consider a specimen that is 100% martensite at room temperature. When the temperature of the SMA actuator is increased to a temperature of A_{s}, the martensite → austenite transformation would occur, when the temperature reaches A_{f}, then the transformation is finished and the martensitic fraction is zero. However, when the temperature is decreased below M_{s}, the reverse martensite → austenite transformation would occur, when the temperature is decreased to M_{f}, the martensitic fraction is 1, the specimen would recover its original shape.

(i) Martensitic fraction from M_f to M_s:

$$\xi = \frac{1-\xi_A}{2}\cos\left[a_M(\theta_S - M_f) - b_M\sigma\right] + \frac{1+\xi_A}{2}$$
$$M_f \leqslant \theta_S \leqslant M_s \tag{11}$$

(ii) Martensitic fraction from A_s to A_f:

$$\xi = \frac{1}{2}\xi_M\left\{\cos\left[a_A(\theta_S - A_s) - b_A\sigma\right] + 1\right\}$$
$$A_s \leqslant \theta_S \leqslant A_f \tag{12}$$

The material constants ξ_A, ξ_M are the martensite fraction before phase transformation begins and a_M, a_A, b_M and b_A are material constants in terms of the transition temperatures, A_s, A_f, M_s and M_f as follows:

$$a_M = \pi(M_s - M_f) \tag{13}$$
$$b_M = a_M/c_M \tag{14}$$
$$a_A = \pi/(A_f - A_s) \tag{15}$$
$$b_A = a_A/c_A \tag{16}$$

where c_M and c_A are material constants related to the influence of stress on the phase transformation. In this simulation, the value of stress (σ) is supposed to be zero due to no external load on the SMA actuator. The martensite fraction ξ_A and ξ_M can be set to be zero and 1, respectively.

For the SMA, the shape deformation F is given by

$$dF = F_{max}\,d\xi \tag{17}$$

where F_{max} is the maximum shape deformation which is determined by the structure of actuator. Based on Eqs. (11), (12) and (17), the governing function of SMA actuator's behavior is shown in Eq. (18).

Table 1
Properties of the materials

Materials	ρ (g/cm^3)	C_p (J/kg K)	λ (W/mK)	υ (m^2/s)
NiTi alloy	6.2	500	15	
Water (283 K)	0.9997	4191	0.574	1.306×10^{-6}
Water (353 K)	0.9718	4195	0.674	0.365×10^{-6}

$$\frac{dF}{F_{max}\,d\theta_S} = \frac{d\xi}{d\theta_S} = \begin{cases} 0, & M_f \geqslant \theta_S \\ \frac{\pi a_M}{8}\sin[a_M(\theta_S - M_f)], & M_f \leqslant \theta_S \leqslant M_s \\ 0, & M_s \leqslant \theta_S \leqslant A_s \\ \frac{\pi a_A}{8}\sin[a_A(\theta_S - A_s)], & A_s \leqslant \theta_S \leqslant A_f \\ 0, & A_f \leqslant \theta_S \end{cases} \tag{18}$$

The initial conditions are:

$$u(0, x, y) = v(0, x, y) = 0, \qquad \theta(0, x, y) = 298\ \text{K} \tag{19}$$

The jet velocity varies from 0.5 to 4 m/s, L/D from 5 to 25. The temperature of the liquid-jet is 353 and 283 K alternately at a certain period ranging from 2 to 4 s. In the simulation, both the moving boundary condition and static boundary condition are adopted on the liquid–solid interface. The properties of the materials are shown in Table 1.

3. Experimental apparatus and procedure

The schematic diagram of the experimental apparatus for the jet impingement on the SMA actuator is shown in Fig. 2. The apparatus consists of a water tank, two pumps, two flow meters, a heat exchanger, a heating apparatus, a three-way valve, some water tubes with an inner diameter of 1.0 cm, two electromagnetic valves, a time relay, and a SMA actuator, etc. The jet water is supplied by the pumps. The

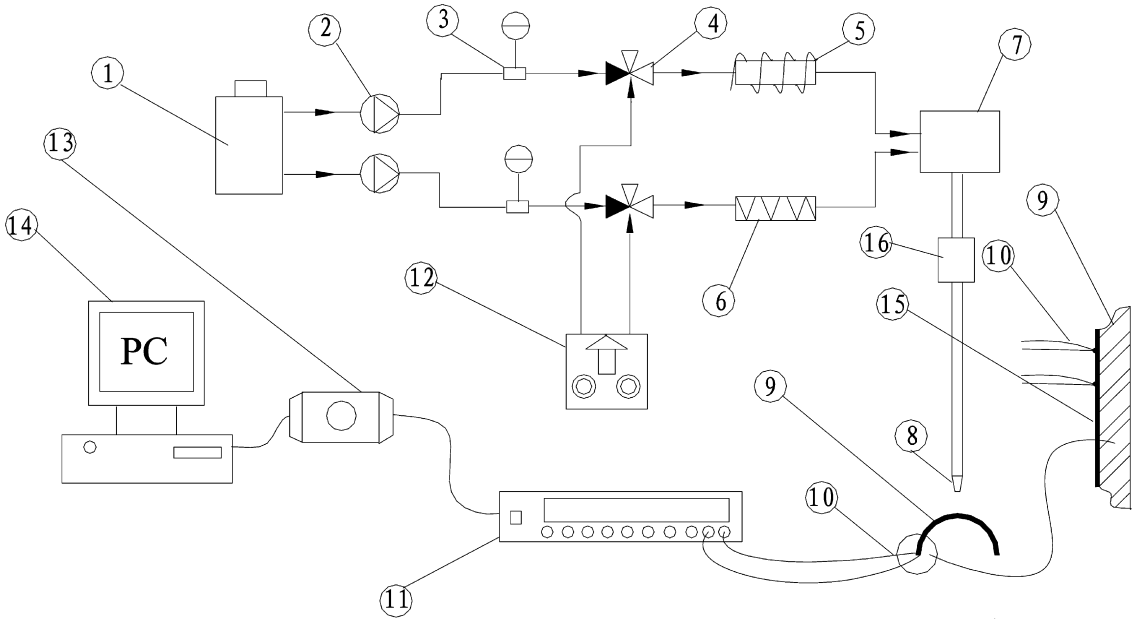

Fig. 2. Schematic diagram of the test apparatus for the jet impingement on the SMA actuator. 1—water tank; 2—pump; 3—flow meter; 4—electromagnetic valve; 5—heating apparatus; 6—cooling apparatus; 7—three-way valve; 8—jet exit; 9—SMA actuator; 10—thermocouple; 11—data collector; 12—time relay; 13—serial-port; 14—computer; 15—silicon resin; 16—water chamber.

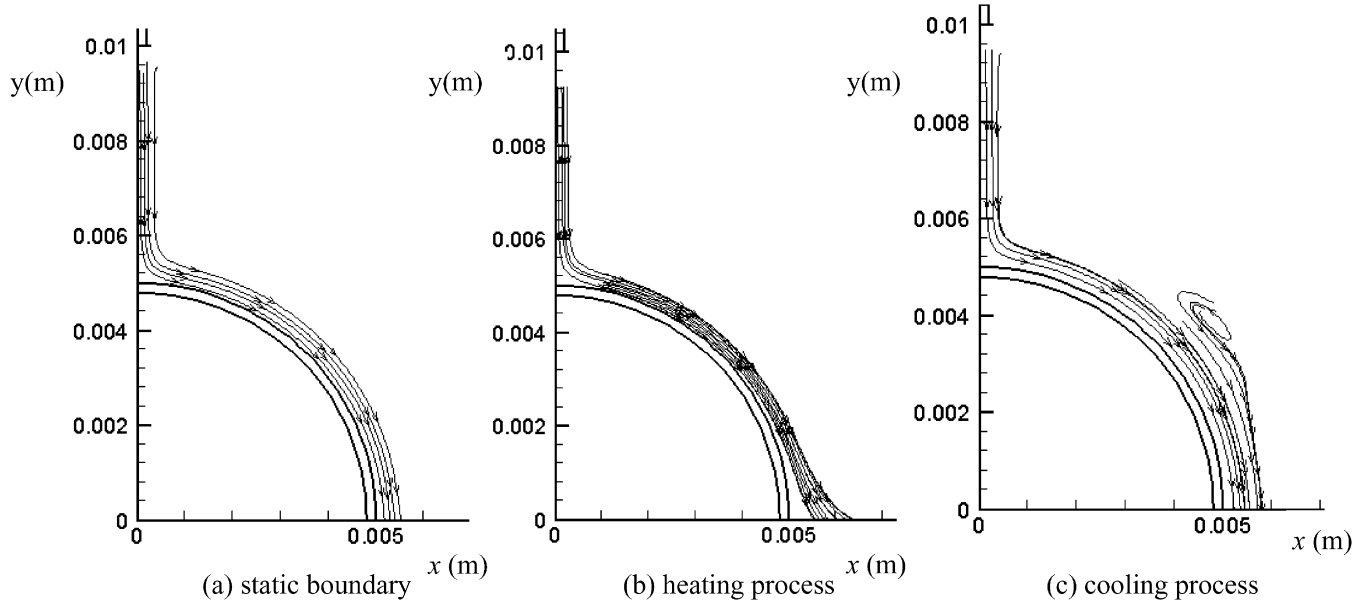

Fig. 3. Flow field of jet impingement on the SMA surface for $L/D = 25$.

heat exchanger is installed to obtain the low temperature water at the nozzle exit; while the heating apparatus made of resistance wire is installed to obtain the high temperature flow. In order to get the constant temperature flow, the generated heat flux in the resistance wire is controlled by the variation of output voltage and calculated by measuring the voltage drop and the electrical current. The electromagnetic valves controlled by regulation of the model of TD2-Y time relay are used to realize the periodic thermal jet flow.

The SMA actuator temperature distribution (θ_S) is measured by chromel-nisiloy thermocouples with 0.1 mm in diameter. Several thermocouples are attached on the backside of the surface along the flow direction. The jet temperatures are measured in the water chamber, mounted between the three-way valve and the jet nozzle exit, with an inner diameter of 1.6 cm to avoid the disturbance of the jet flow at the nozzle exit. The measured temperatures are recorded by a multi-channel QD16 data collector and stored in the personal computer with the model of R232 serial-port. It should be referred that the parameters such as the temperatures of the SMA actuator and the jet fluid are recorded till the system becomes stable, once the work condition is changed.

The SMA actuator of 15.7 mm × 10 mm × 0.2 mm is made of NiTi alloy with an atomic composition of Ti/Ni = 50.5/49.5. In the experiment, the SMA actuator is restricted by some external load in order to keep the safety of the thermocouples. The overall uncertainty of the transient temperature distribution is primarily determined by the influence of the silicon resin membrane and the accuracy of data collector and thermocouples. The uncertainty brought by the membrane between the SMA actuator and the thermocouples is estimated to be about 5%. The accuracy of the chromel-nisiloy thermocouple and the QD16 data collector used to measure the temperature are 0.2% and 0.5%, respectively.

4. Results and discussion

For considering the complicated influence of the jet velocity, jet period, nozzle-to-surface distance and boundary condition on the heat transfer and thermal response of the SMA actuator, the transient temperature distribution, the pressure distribution and the shape deformation of the SMA actuator are numerically and experimentally examined for different conditions.

4.1. Flow feature on the moving SMA surface

The streamline of jet impingement on the moving SMA surface is shown in Fig. 3 for different processes, Fig. 3(a) for the static boundary, Fig. 3(b) for the heating process, Fig. 3(c) for the cooling process for jet velocity 2 m/s and nozzle-to-surface distance $L/D = 25$ numerically. In Fig. 3(a) a regular laminar flow is formed on the SMA surface due to the assumption of the static boundary. It can be seen from Fig. 3(b) that separation on the moving SMA surface is observed for the heating process, because the SMA actuator would bend down in the heating process as shown in Fig. 1. This observation agrees well with that of Justesen [26] and Zhang [27]. From Fig. 3(c), some vortices away from the moving surface are induced, which is different from that of Zhang [27], where the vortices come into being near the surface for the cooling process. The reason could be attributed that the viscous force near the surface is higher than the inertia force for small jet velocity and low motion frequency.

4.2. Pressure distribution on the SMA surface

The effect of jet velocity and moving surface on pressure coefficient $C_p = p/p_{max}$ is shown in Fig. 4(a) and (b) for nozzle-

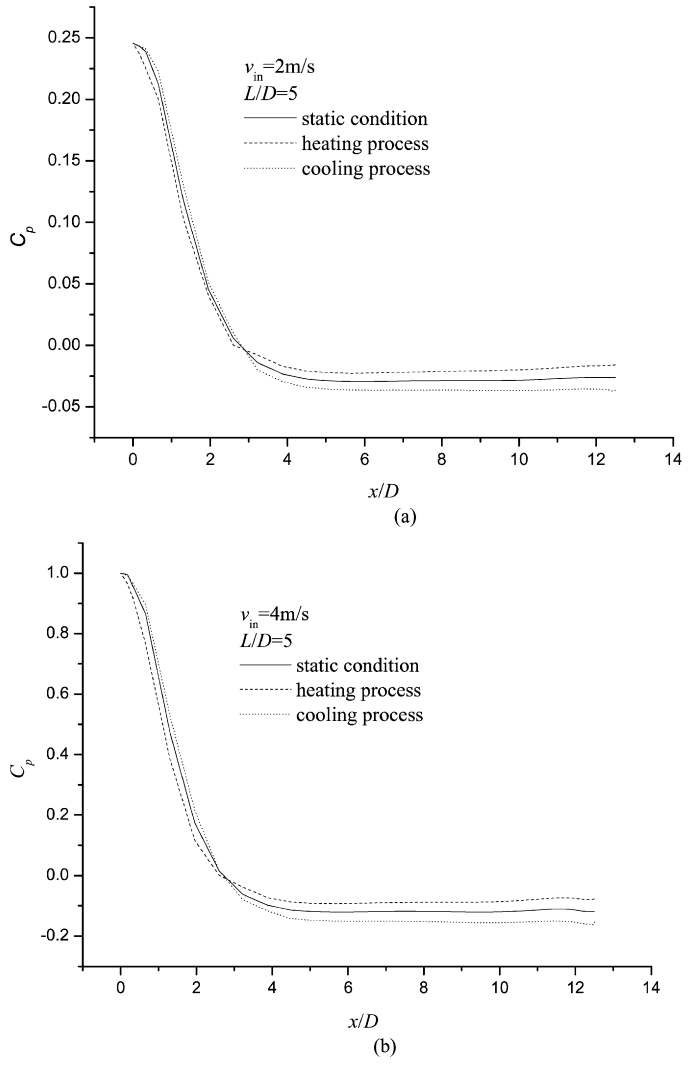

Fig. 4. Pressure distribution for jet impingement on the SMA surface for different velocity.

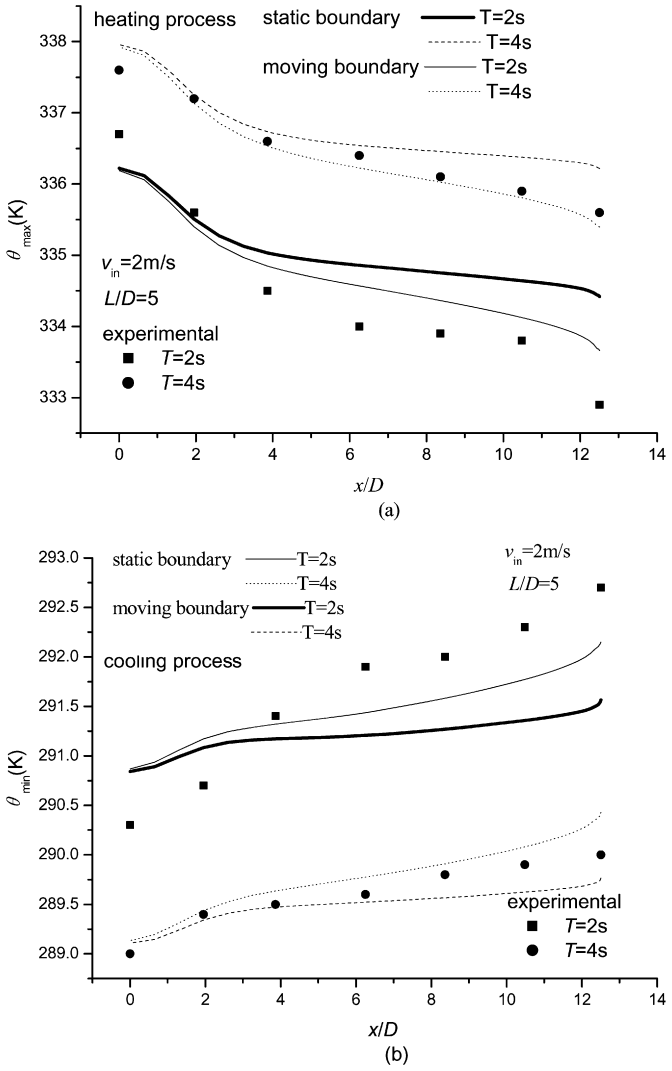

Fig. 5. Effect of jet period on the temperature of the SMA actuator.

to-surface distance ($L/D = 5$) numerically, where p is the pressure on the SMA surface, $p_{\max}$ is the maximum pressure. It is observed from Fig. 4 that the pressure distributions on the moving surface are not only dependent on the jet velocity, which is similar with water jet on the plate by Li and Wu [28], but also dependent on the moving boundary condition of the SMA actuator. At the stagnation point ($x/D = 0$), the velocity is zero, the pressure is equal to the maximum value. A subatmospheric region on the impingement surface was observed with the increase of x/D, similar findings could be obtained in literature by Baydar and Ozmen [29]. In the former portion of the curves, the pressure for the cooling process is higher than that for the static condition, the SMA actuator would move upwards, which is in the opposite direction with the flow, the velocity decreases more quickly, which is reverse for the heating process. While in the latter portion of the curves, in the subatmospheric region, the pressure for the heating process is higher than that for the static condition because of the occurrence of the separation as shown in Fig. 3.

4.3. Effect of jet period, velocity and L/D on the temperature distribution

The temperature of the SMA actuator would change at a certain frequency regularly after several minutes of periodic thermal jet impingement. Figs. 5–7 only show the maximum and minimum results numerically and experimentally, after the situation of the temperature fluctuation of the SMA actuator becomes stabilization, noted that the maximum results represent the temperatures of the SMA actuator at the time when the heating process has finished, the minimum results represents the temperatures when the cooling process has finished.

The effect of jet period on the temperature of the SMA actuator is plotted in Fig. 5 for $T = 2$ s, $T = 4$ s, and $v_{\text{in}} = 2$ m/s numerically and experimentally. The maximum temperature for $T = 4$ s is higher than that for $T = 2$ s; however, the minimum temperature for $T = 4$ s is lower than that for $T = 2$ s. The maximum temperature exhibits a decreasing trend along the forward direction of x/D both for the static and moving boundary conditions. The distribution of the minimum temperature is just reverse to the maximum temperature. The temperature at

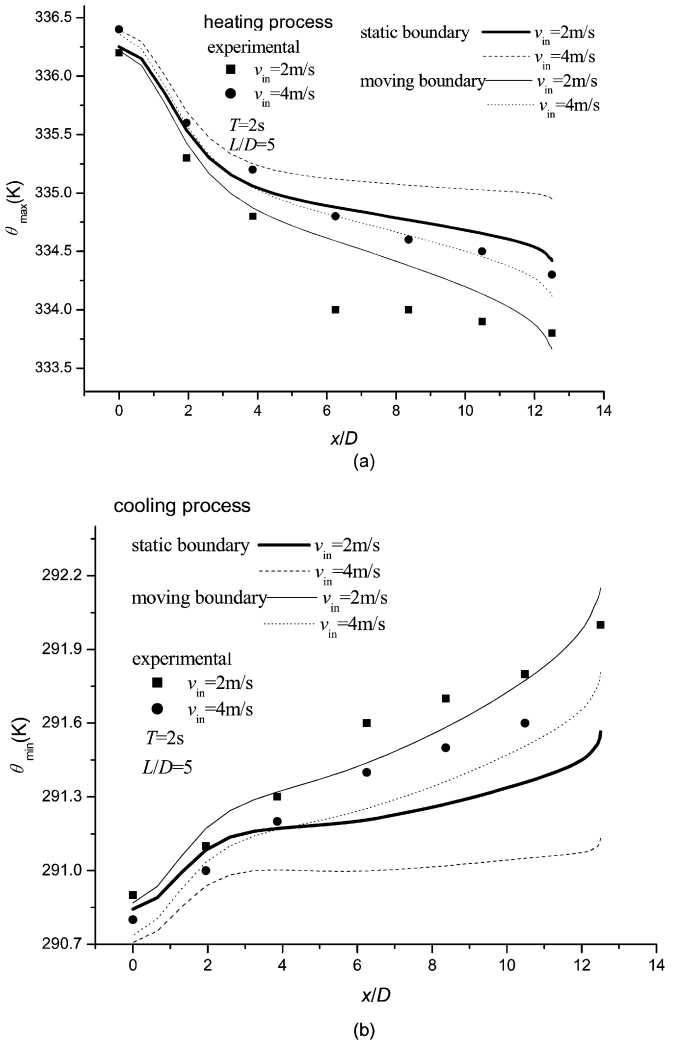

Fig. 6. Effect of jet velocity on the temperature of the SMA actuator.

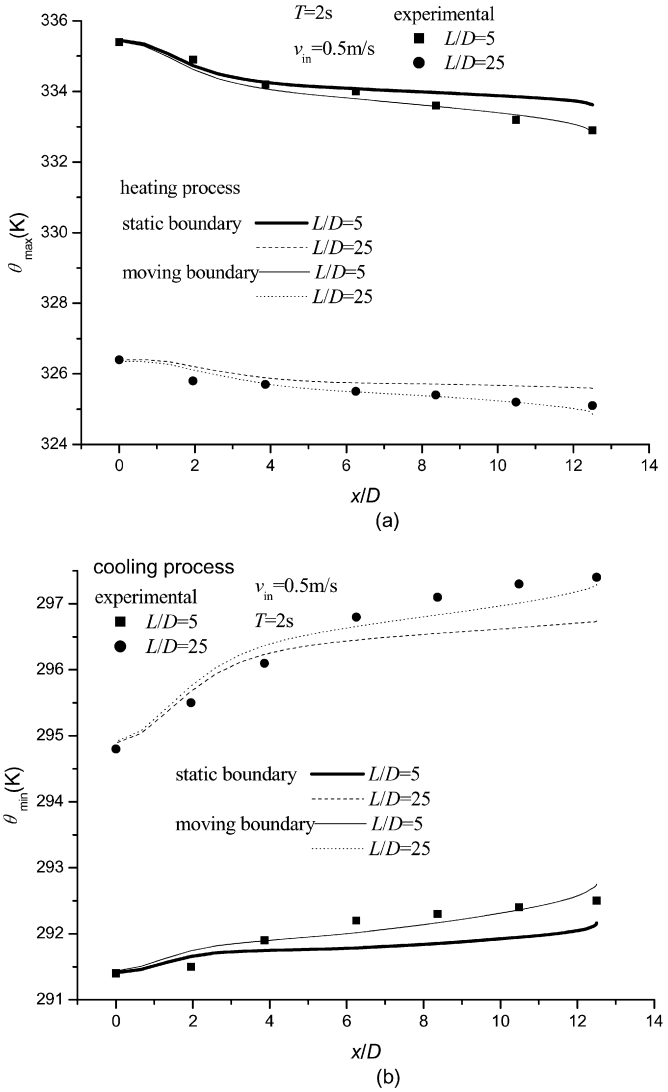

Fig. 7. Effect of jet L/D on the temperature of the SMA actuator.

$x/D = 0$ for moving boundary condition is almost the same with that for static boundary condition. This is because no additional disturbance occurred for little flutter at this point. The temperature difference between static boundary condition and moving boundary condition increases along the forward of x coordinate. This is attributed to the separation and disturbance intensification along the flow direction for increasing extent of flutter, as shown in Fig. 3.

The temperature distributions of the SMA actuator for various jet velocities are shown in Fig. 6 for $T = 2$ s and $L/D = 5$ numerically and experimentally. Fig. 6(a) and Fig. 6(b) show the maximum and the minimum temperature at periodic thermal boundary condition, respectively. The maximum temperature increases with the increase of the jet impingement velocity and the minimum temperature decreases with the increase of the jet impingement velocity. This reason is that an increase of the jet velocity would lead to a stronger disturbance and heat transfer. It can also be seen from Fig. 6 that the influence of the jet velocity on the temperature distribution is not pronounced, this is because the jet fluid and SMA actuator can reach the thermal balance instantaneously due to higher heat transfer coefficient of jet impingement.

Fig. 7 shows the effect of L/D on the temperature distribution of the SMA actuator numerically and experimentally. It should be indicated from Fig. 7 that the influence of L/D on the temperature distribution is more pronounced than the other two factors referred above. This is because that the jet fluid has a stronger heat transfer for longer nozzle-to-surface distance, before it reaches the surface of the SMA actuator.

4.4. Effect of jet period, velocity and L/D on the shape deformation

One of the most important characteristics for SMA is that it can flutter regularly with its temperature fluctuation. In order to investigate the effect of the jet velocity, period and L/D on the shape deformation, a dimensionless ratio $F/F_{\max}$ is presented in Fig. 8 for $L/D = 5$ and Fig. 9 for $v_{\text{in}} = 2$ m/s numerically, As shown in Fig. 8 and Fig. 9, $F/F_{\max}$ increases with the increase of the jet velocity and period, decreases with the increase of L/D. This can also be explained by the temperature distribution of the SMA actuator in Figs. 5–7. In the range

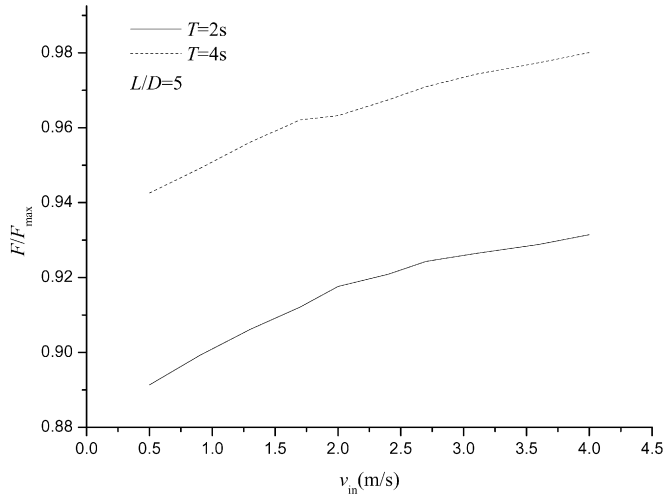

Fig. 8. Effect of jet velocity on the shape deformation of the SMA actuator.

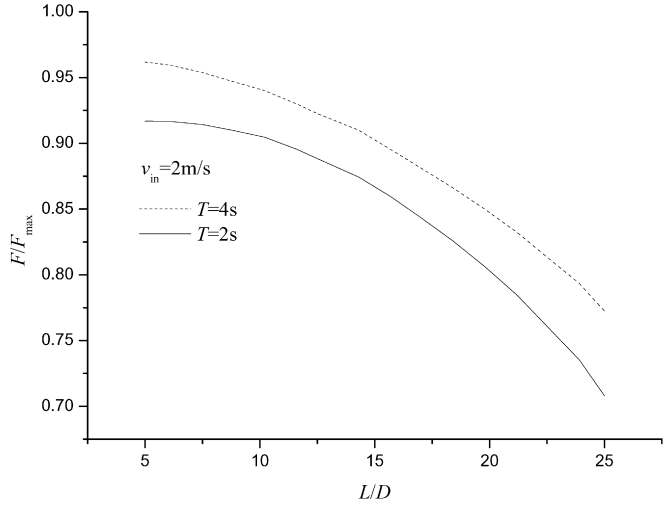

Fig. 9. Effect of nozzle-to-surface distance on the shape deformation of the SMA actuator.

of the parameters conducted by the numerical simulation, the SMA actuator exhibits good shape deformation performance, so we can say that the SMA actuator not only can be actuated by liquid-jet impingement but also can meet the demands of high actuated frequency. Considered the ratios of the generating force to the weight, SMA would play an important role in design of the MEMS in the future.

5. Conclusions

The experimental study and numerical simulation have been carried out to investigate the effects of the velocity, nozzle-to-surface distance, the jet period and moving boundary condition on the flow and temperature field of the SMA actuator. In this paper, a new moving boundary condition depending on a constitutive equation of the SMA by Liang and Logers [24] was disposed at the periodic thermal boundary condition and there was also a conjugated heat transfer at solid–fluid interface between the jet water and the SMA actuator. Results were generated as follows:

(1) The flow field on the moving surface exhibits different characteristics than that on the static surface. Separation on the moving SMA surface is observed for the heating process, some vortices away from the moving surface are induced for the cooling process.
(2) The pressure distributions on the impingement moving surface are not only dependent on the jet velocity, but also dependent on the motion of the SMA actuator. For the cooling process, the pressure curve is higher than that for the static condition, while it is just reverse for the heating process in the former portion; in the latter portion, the pressure distribution shows an opposite regularity to the former portion.
(3) Rapid heat transfer occurs between the jet fluid and SMA actuator, after the jet impingement began. The maximum temperature increases with the increase of the jet velocity and period, the minimum temperature decrease with the increase of the jet velocity and period. The influence of L/D on the temperature distribution is more pronounced than the jet velocity and period.
(4) The SMA actuator can flutter at a certain period and the SMA actuator exhibits good shape deformation performance.

Acknowledgements

The authors gratefully acknowledge financial support by the National Science Foundation of China under the grant No. 50646024.

References

[1] J.J. Gill, K. Ho, G.P. Carman, Three-dimensional thin-film shape memory alloy microactuator with two-way effect, Journal of Microelectromechanical Systems 11 (2002) 68–78.
[2] Z.G. Wang, X.T. Zu, X.D. Feng, Effect of thermomechanical treatment on the two-way shape memory effect of NiTi alloy spring, Materials Letters 54 (2002) 55–61.
[3] C. Invernizzi, P. Iora, Heat recovery from a micro-gas turbine by vapour jet refrigeration systems, Applied Thermal Engineering 25 (2005) 1233–1246.
[4] S.T. Wang, G.T. Feng, Z.Q. Wang, Numerical simulation of coolant jet structure in turbine cascade, Journal of Aerospace Power 15 (2000) 274–277.
[5] Q.G. Chen, Z. Xu, Y.J. Zhang, Advances in numerical studies of turbulent impinging jet flow and heat transfer, Advances in Mechanics 32 (2002) 92–108.
[6] T.T. Guo, S.H. Li, Z. Xu, Numerical simulation of three-dimensional turbulent jets in crossflow, Proceedings of the CSEE 23 (2003) 191–195.
[7] P. Yu, W.X. Sun, Numerical analysis on the heat transfer performance of CPU heat sink cooled by vertical uniform jet, Journal of Engineering Thermophysics 23 (2003) 415–418.
[8] A. Inoue, A. Ui, Y. Yamazaki, et al., Studies on cooling by two-dimensional confined jet flow of high heat flux surface in fusion reactor, Nuclear Engineering and Design 200 (2000) 317–329.
[9] A. Inoue, A. Ui, Y. Yamazaki, et al., Studies on a cooling of high heat flux surface in fusion reactor by impinging planar jet flow, Fusion Engineering and Design 51–52 (2000) 781–787.
[10] A. Inoue, T. Tanno, M. Takahashi, et al., Two-dimensional impinging jet cooling of high heat flux surfaces in magnetic confinement fusion reactors, Fusion Engineering and Design 28 (1995) 81–89.
[11] J.S. Bintoro, A. Akbarzadeh, M. Mochizuki, A closed-loop electronics cooling by implementing single phase impinging jet and mini channels heat exchanger, Applied Thermal Engineering 25 (2005) 2740–2753.

[12] J. Walker, K. Gabriel, Thin-film processing of TiNi shape memory alloy, Sensors and Actuators A 21–23 (1990) 243–246.

[13] O.K. Rediniotis, D.C. Lagoudas, L.N. Wilson, Development of a shape-memory-alloy actuated biomimetic hydrofoil, Journal of Intelligent Material Systems and Structures 13 (2002) 35–49.

[14] K.T. Lau, L.M. Zhou, X.M. Tao, Control of natural frequencies of a clamped–clamped composite beam with embedded shape memory alloy wires, Composite Structure 58 (2002) 39–47.

[15] J.V. Humbeeck, Damping capacity of thermoelastic martensite in shape memory alloys, Journal of Alloys and Compounds 355 (2003) 58–64.

[16] A. Baz, A. Tempia, Active piezoelectric damping composites, Sensors and Actuators A 112 (2004) 340–350.

[17] E. Makino, T. Mitsuya, T. Shibata, Fabrication of TiNi shape memory micropump, Sensor and Actuators A 88 (2001) 256–262.

[18] D.D. Shin, K.P. Mohanchandra, G.P. Carmen, Development of hydraulic linear actuator using thin film SMA, Sensor and Actuators A 119 (2005) 151–156.

[19] M. Kohl, B. Krevet, E. Just, SMA microgripper system, Sensors and Actuators A 97–98 (2002) 646–652.

[20] A. Bhattacharyya, M.G. Faulkner, J.J. Amalraj, Finite element modeling of cyclic thermal response of shape memory alloy wires with variable material properties, Computational Materials Science 17 (2000) 93–104.

[21] M.M. Ghomshei, N. Tabandeh, A. Ghazavi, Nonlinear transient response of a thick composite beam with shape memory alloy layers, Composites B 36 (2005) 9–24.

[22] D.C. Lagoudas, A. Bhattacharyya, Modeling of thin layer extensional thermoelectric SMA actuators, International Journal Solids and Structures 35 (1998) 331–362.

[23] M. Rohde, A. Schüssler, On the response-time behaviour of laser micromachined NiTi shape memory actuator, Sensors and Actuators A 61 (1997) 463–468.

[24] C. Liang, C.A. Logers, One-dimensional thermomechanical constitutive relations for shape memory materials, Journal of Intelligent Material Systems and Structures 1 (1990) 207–234.

[25] L.X. Zhang, G.X. Hu, Experimental study of heat transfer characteristics with impinging jet at curved surface, Journal of Chemical Industry and Engineering 56 (2005) 1409–1412.

[26] P. Justesen, A numerical study of oscillating flow around a circular cylinder, Journal of Fluid Mechanics 222 (1991) 157–196.

[27] H.L. Zhang, X. Zhang, Flow structure analysis around an oscillating circular cylinder at low *Kc* number: a numerical study, Computer & Fluids 26 (1997) 83–106.

[28] D.S. Li, J.G. Wu, Study on numerical simulation of plane jet, Energy for Metallurgical Industry 21 (2001) 42–45.

[29] E. Baydar, Y. Ozmen, An experimental and numerical investigation on a confined impinging air jet at high Reynolds numbers, Applied Thermal Engineering 25 (2005) 409–421.